Wavelet/PSO-Based Segmentation and Marker-Less Tracking of the Gallbladder in Monocular Calibration-free Laparoscopic Cholecystectomy

Haroun Djaghloul
University of Ferhat Abbes - Setif 1, Algeria

Jean-Pierre Jessel
IRIT, Institut de Recherche en Informatique de Toulouse, France

Mohamed Batouche
University of Constantine 2, Algeria

Abdelhamid Benhocine
University of Ferhat Abbes - Setif 1, Algeria

***Abstract*—This paper presents an automatic segmentation and monocular marker-less tracking method of the gallbladder in minimally invasive laparoscopic cholecystectomy intervention that can be used for the construction of an adaptive calibration-free medical augmented reality system. In particular, the proposed method consists of three steps, namely, a segmentation of 2D laparoscopic images using a combination of photometric population-based statistical approach and edge detection techniques, a PSO-based detection of the targeted anatomical structure (the gallbladder) and, finally, the 3D model wavelet-based multi-resolution analysis and adaptive 2D/3D registration. The proposed population-based statistical segmentation approach of 2D laparoscopic images differs from classical approaches (histogram thresholding), in that we consider anatomical structures and surgical instruments in terms of distributions of RGB color triples. This allows an efficient handling, superior robustness and to readily integrate current intervention information. The result of this step consists in a set of point clouds with a loosely gradient information that can cover various anatomical structures. In order to enhance both sensitivity and specificity, the detection of the targeted structure (the gallbladder) is based on a modified PSO (particles swarm optimization) scheme which maximizes both internal features density and the divergence with neighboring structures such as, the liver. Finally, a multi-particles based representation of the targeted structure is constructed, thanks to a proposed wavelet-based multi-resolution analysis of the 3D model of the targeted structure which is registered adaptively with the 2D particles generated during the previous step. Results are shown on both synthetic and real data.**

Keywords*—Medical image segmentation; monocular laparoscopic cholecystectomy; deformable structures tracking; gallbladder segmentation and tracking; markerless augmented reality; wavelets; particles swarm optimisation; minimally invasive surgery (MIS); computer aided surgery (CAS)

I. Introduction

Medical augmented reality consists in a set of techniques that allow the visualization in transparency of anatomical and pathological structures reconstructed pre-operatively using medical images (IRM, CT-Scan) in the surgeon's field of view. Augmented reality provides contextual information in an intuitive and easily implemented display [1], [2]. However, one of the major challenges remains in the limits augmented reality use in clinical laparoscopic abdominal surgery is the difficulty of marker-less immediate and precise registration of preoperative deformable 3D models of digestive organs reconstructed using medical images such as MRI or CT-Scan on the intra-operative laparoscopic view.

Augmented reality allows the enhancement of perceptual capabilities of surgeons during the intervention directly on their filed of view of the intervention or projected on the patient. Because of the rigidity of manipulated anatomical structures, many augmented reality systems have been integrated in the operative rooms especially for orthopedic and neurosurgery. However, in the case of highly deformable anatomical structures as in the case of abdominal surgery, many challenges have been encountered due to the difficulty to precisely track and register the targeted anatomical structures. On the other hand, the massive adoption of minimally invasive surgery techniques even with their advantages have introduced other drawbacks such as the lack of tactile sensation, the limitation of the intervention field of view and the inversion of surgical instruments gesture orientations. These problems can be overcome, thanks to the use of augmented reality.

A. Motivation and Proposition

In this study, we focus on the segmentation and marker-less tacking of the gallblader during monocular minimally invasive laparoscopic cholecystectomy intervention with no camera calibration parameters available. Cholecystectomy is the standard procedure for surgical treatment of gallbladder diseases mainly for symptomatic cholelithiasis (gallstones). It consists in the ablation of the gallbladder and its extraction from the abdomen of the patient. In the case of minimally invasive surgery or laparoscopic surgery, a set of special surgical instruments are inserted into the abdominal cavity of the patient through a small incisions.

Cholecystectomy is the first surgical intervention in the United States with more than a half million operations done each year. Since the first cholecystectomy of Langenbuch [3], [4]. Indeed, cholelithiasis is an extremely common gallbladder condition, generally reaching the quart of the population beyond 50 years with one of three women and one of five men that have or will have it. Cholecystectomy consists in the complete removal of the gallbladder with different techniques such as open, laparoscopic [3], SILS or NOTES [5], [6] procedures. The video-assisted laparoscopic cholecystectomy

is currently the gold standard technique with more than 98% of performed interventions [7]–[10].

Digestive organs are highly deformable leading to certain displacement of any physical radio opaque markers between preoperative and intra-operative acquisitions. Moreover, inter and intra-patient geometric and anatomical variability and the great complexity of intra-abdominal surgical environment caused by dissection and bleeding. The preoperative patient specific 3D model can only be used as initial solution for anatomical and pathological structures detection and tracking. Therefore, the surgical intervention cannot be safe and precise in this such complex context of monocular laparoscopic cholecystectomy without handling and tracking the deformation of the primary manipulated anatomical structure which is the gallbladder.

Here, we propose a method for tracking digestive organs on the view of previous medical augmented reality systems in laparoscopic cholecystectomy. Thus, the proposed method can be used as a priori step to markers-based registration systems to align coarsely the patient CT/MRI model reconstructed before the surgical intervention. In other side, the method can be used intra operatively to track targeted organs or surgical instruments with partially occluded or totally invisible markers. Therefore, we propose a new nearly-automatic statistical color model construction method and its application to the pixel-wise anatomical structures detection and tracking in the context of the laparoscopic cholecystectomy.

B. Paper Organisation

The rest of the paper is organized as follows. In Section 2, we outline the fundamentals of a standard laparoscopic cholecystectomy procedure and its operative workflow. Then, we review state of the art of the methods used to handle deformable objects detection and tracking mainly used in laparoscopic medical augmented reality systems and discussing their capabilities and limitations. In Section 4, we describe materials and provide the mathematical formula and the necessary background and implementation of the proposed method. In Section 5, we present experimental results and the overall characteristics of the method. Section 6 presents our conclusions, potential applications of the proposed methods and perspectives.

II. Medical Background

According to the common and standard ports installation and intervention workflow providing optimal results [3], [11], [12], the basic laparoscopic cholecystectomy intervention according to the European operating technique begins with achieving a perfect exposure of the right sub-hepatic region. Then, the surgeon uses the inserted laparoscopic camera to detect and identify all anatomical structures in the abdominal cavity. The next major steps are mainly the dissection of Callot's triangle, dissection/clipping and division of the cystic artery and duct. Finally, a complete removal of the gallbladder is achieved by dissecting the gallbladder bed with the liver. In most cases, computer-assisted surgery workflow models are created manually, which is a time consuming process that might suffer from a personal bias. In their work [13], Blum et al. presented a graphical user interface based on an approach for automatic workflow mining using ten process logs, each describing a single instance of a laparoscopic cholecystectomy, to build a Hidden Markov Model (HMM) with embody statistical information concerning aspects like duration of actions or tool usage during the surgery. In Fig. 1, we outline our proposition for standard laparoscopic cholecystectomy workflow model based on six coarse main steps.

From a topographical anatomy point of view, the principal anatomical structures of the right upper quadrant that have to be explored, during the intra-operative detection and identification step, in the operating field of view are the liver, the gallbladder, the round ligament, the stomach, the duodenum, the transverse colon, the lesser omentum, the hepatic flexure and the greater omentum. In our context, the most important anatomical structure is the gallbladder and its vascular supply. The major gallbladder anatomical structures are the fundus, the body, the infundibulum, the cystic duct, the common hepatic duct and the common bile duct. The vascular supply elements are mainly the cystic artery, the Mascagni lymph node, the proper hepatic artery, the abdominal aorta, the portal vein and gastro-duodenal artery. More details about sub-hepatic anatomical structures can be found in medical literature. In this paper we base our work on the Foundational Model of Anatomy (FMA) ontology to guide the anatomical structures modeling and recognition.

III. Related Works

Tracking real objects is an important topic in computer vision. Many methods for tracking real objects have been proposed in the literature. In this paper, we are mainly interested to the visual tracking of non-rigid objects. Several methods have been proposed with applications to different domains [14]. However, few clinical results exist for deformable abdominal organs tracking in laparoscopic cholecystectomy. Medical tracking systems for digestive surgery can be classified into two categories, namely, optical and hybrid systems. In their work [15], Nicolau et al. proposed a low cost and accurate guiding system for laparoscopic surgery with validation on abdominal phantom. The system allows real time tracking of surgical tools and registration at 10 Hz of the preoperative patient CT/MRI reconstructed model with accuracy tracking of instrument tip close to 1.5 mm and endoscopic overlay error under 1.0 mm. The system is totally based on the AR-Toolkit [16], [17] markers and patterns use for both patient model registration and surgery instruments tracking. To register abdominal markers the method minimize the Extended Projective Points Criterion (EPPC) instead of the Standard Projective Points Criterion (SPPC) because of its error support either of 2D image or 3D CT-Scan data [18], [19]. Validation of the criterion has mainly been made for radio-frequency surgery without abdominal gas insufflation. Accurate tracking and registration of such markers in real intra-abdominal laparoscopic surgery is very difficult because of the digestive organs deformation and the pneumoperitoneum establishment [3], [20]. Feuerstin et al. [21] use multiple optical and electromagnetic tracking systems to determine the position and orientation of intra-operative imaging devices (mobile C-arm, laparoscopic camera and flexible ultrasound) allowing direct superimposition of acquired patient data in minimally invasive liver resection. To our knowledge, there is

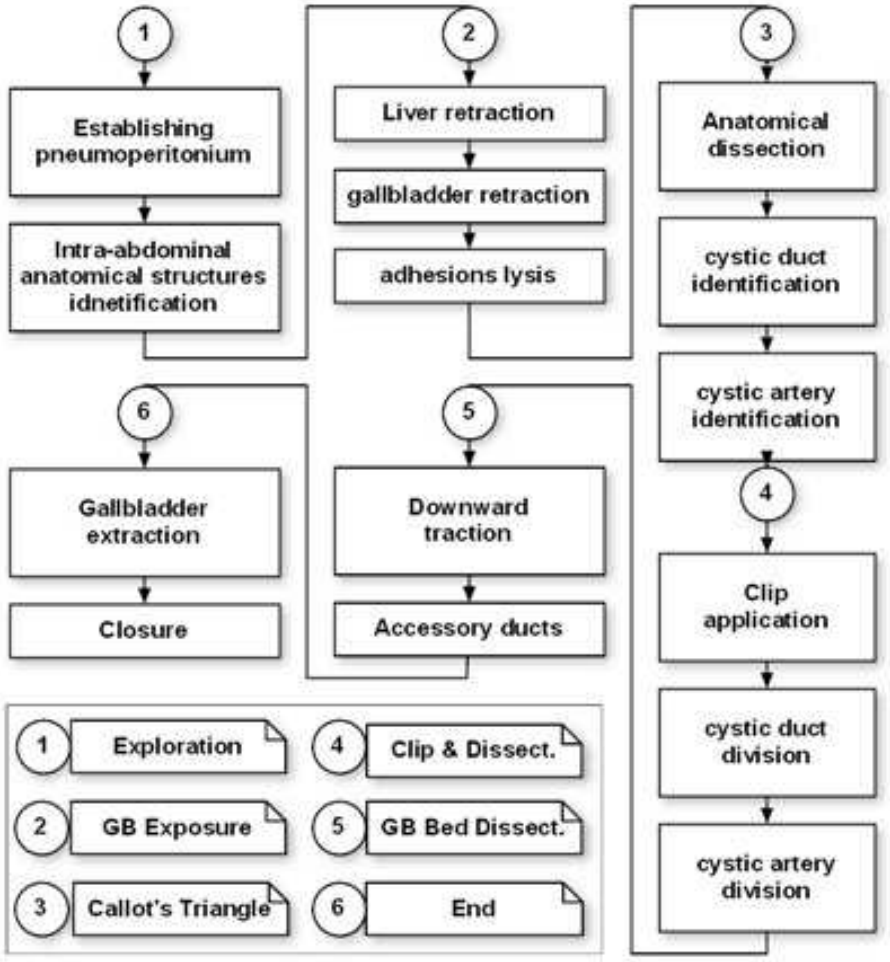

Fig. 1. Standard laparoscopic cholecystectomy procedure.

no clinically approved automatic marker-less tracking systems of the gallbladder during laparoscopic cholecystectomy.

IV. Proposed Method

In this section, we describe the proposed method for the segmentation and tracking of the gallbladder using photometric features. Therefore, we need to build a color model of gallbladder as well as the other neighboring anatomical structures. To achieve this goal with minimal user interaction, we propose the following straightforward method that can take into account the patient anatomy variability and the standard intervention workflow according to the European operative room set-up and common standard installation of the patient in the operative room during the intervention.

In Fig. 2, we show the global architecture of the proposed system for the application of the pre-operative statistical color model in anatomical and pathological structures detection and tracking tasks. Indeed, the system allows on-line enhancement of the initial pre-operative color model using the intra-operative laparoscopic intervention video.

In the following sub-sections we describe the off-line statistical anatomical color model construction. We first build a general histogram density using a set of high quality captured videos and photos of standard laparoscopic cholecystectomy interventions available at the World Wide Web. The images have 240 x 320 RGB coded pixels with 256 bins per channel (24 bits per pixel). Each video sequence is acquired at a frame rate of 30 Hz. We remove manually from the video training dataset all frames that are not relevant, such as tutorial text and operative room presentation, focusing only on inner abdominal laparoscopic camera photos. We have a final set of 16735 colored laparoscopic images, resulting in a training dataset containing more than one billion pixels.

A. Pre-operative Anatomical Color Model

This first step allows to automatically extract both important anatomical structures and surgical instruments blobs that are directly visible using the laparoscope camera. The first laparoscopic image of each training intervention video is captured and segmented manually into four main regions (liver, gallbladder, surgical instruments and other). Other region contains the pixels of remaining anatomical or pathological structures that are not segmented manually and with no impact on the following 3D model registration step. According to the cholecystectomy intervention workflow step (t), we construct for each anatomical region (i) a statistical color model using a histogram with 256 bins per channel in the RGB color space.

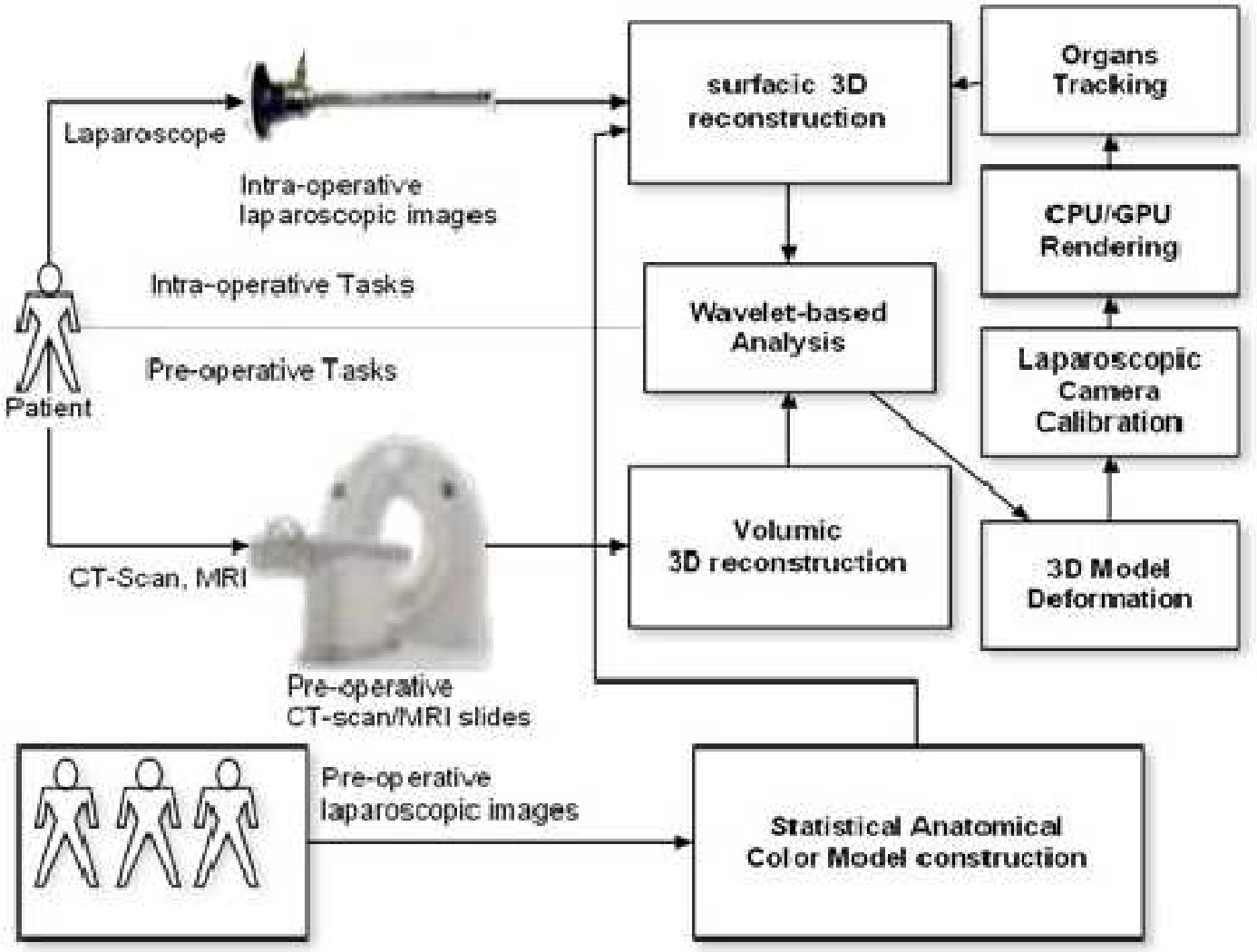

Fig. 2. A schematic illustration of the proposed method.

Each color vector (x) is converted into a discrete probability distribution in the manner:

$$P_{i,t}(x) = \frac{c_{i,t}(x)}{\sum_{j=1}^{N_{i,t}} c_{i,t}(x_j)}, t = t_1 \dots t_6,\ i = 0 \dots S_t\,. \quad (1)$$

where $c_{i,t}(x)$ gives the count in the histogram bin representing the *rgb* color triplet (x) and $N_{i,t}$ is the total count of the *rgb* histogram entries returned by the histogram bins number of the structure region (i) during the intervention step (t). the number of structures (anatomical, pathological or surgical instruments) S_t varies according to the procedure step and the priori knowledge-based patient-specific data. To ensure a generic color model construction, it is important to fix the steps and structures number for the whole training data set. In this study and according to the European standard and common laparoscopic cholecystectomy installation and intervention workflow described in section 2, the number of structures classes is limited to four ($S_t = 4$) and surgical steps to six ($t_1 =$ '$exploration...$'). The class structure $i = 0$ contains the histogram bins with corresponding *rgb* triples which are not included in construction of the previous color model. In practice, the step (t) denotes a time interval represented by the sequence of laparoscopic images of the same intervention $t = \left[I^t_{v,1} \dots I^t_{v,n}\right]$ in the different videos (v) that compose the training data set.

Several mathematical morphological operators are used to eliminate even noise small regions. The determination of major blobs can be performed thanks to the application of connected component labeling. For each anatomical blob we compute statistics such as centroids coordinates, blob area and probabilities of each RGB triple associated to each anatomical structure.

Once the laparoscopic images of the intervention were prepared, different statistical features and properties are extracted. First, we scan each image in the training dataset for all color model features. In Table I, we give some statistical properties of one the laparoscopic cholecystectomy intervention videos used in our study.

Fig. 3 shows the evolution of the RGB histogram bins count over the 16735 frames of the video training dataset.

TABLE I. GLOBAL TRAINING DATASET HISTOGRAM BINS STATISTICS

Feature	*RGBTriplet*	*Red*	*Green*	*Blue*
Mean	1997	31	63	31
Median	2024	32	64	32
Min	61	21	41	20
Max	3245	32	64	32
Standard deviation	499	0	1	0
Total count	10017	32	64	32

We can observe that each laparoscopic image can contains at most 10017 RGB color triplets over all the video sequence. therefore, the RGB histogram is mostly empty with 99,94% of the RGB triples that are not used.

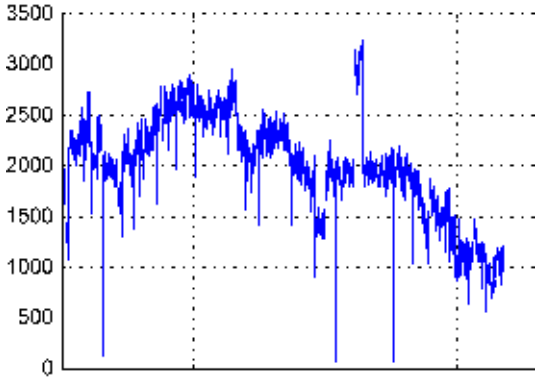

Fig. 3. Evolution of RGB bins count in video training dataset.

In Fig. 4, we can see the spatial distribution of a given color model feature within the laparoscopic image of the gallbladder. One can observe that the same is located over different regions that can belong to different anatomical structures or surgical instruments.

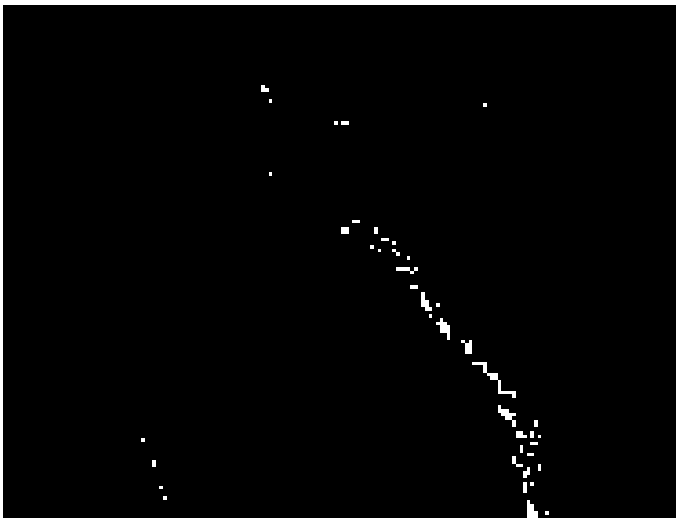

Fig. 4. Spatial distribution of an RGB color triplet in a single laparoscopic image.

The only application of the anatomical color and spatial model using the criteria given above can lead to a course segmentation of the laparoscopic image with a considerable number of artifacts as shown in Fig. 5.

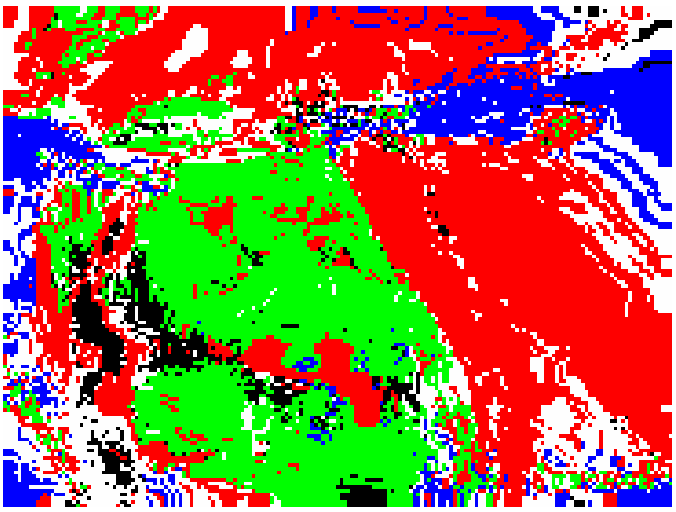

Fig. 5. Detection of anatomical structures using the proposed color model.

The result shown in Fig. 5 confirms the need of additional steps to enhance the segmentation and thus detection result of the gallbladder and surrounding anatomical structures such as the liver. These necessary steps are described in the following subsections given below.

B. Proposed Wavelet for Multi-resolution Tree of Spheres Modeling of Anatomical Structures

In this section, we propose a new multi-resolution analysis of 3D objects modeled as a set of elementary non intersected particles defined by their centers and rays. The virtual model of the anatomical structure is subdivided into a set of spheres. We call this representation the tree of spheres (TOS) model. Here, the closest greatest sphere to the preoperative 3D model gravity center represents the TOS model root or simply the TOS root. The TOS root is used during the first step of the 2D/3D registration between the preoperative reconstructed TOS model and the PSO-based gallbladder detection particles (PSO-DP). The establishment of a correspondence between the TOS root and the PSO-DPs allows to maintain a certain level of stability during deformable registration along the whole laparoscopic intervention video. The TOS root represents the coarsest resolution level of the virtual model of the tracked anatomical structure (the gallbladder).

We suppose that S^j is the TOS at the resolution level (j). We have:

$$S^j = \left[S_{j,1} S_{j,2} \dots S_{j,i} \dots S_{j,n_j}\right]^t \tag{2}$$

where $S_{j,i}$ is the i^{th} sphere of the virtual model at the resolution (j) and n_j is the length of the spheres chain at the resolution level (j) denoting its number of spheres. The initial resolution level is S^0 and the coarsest one is S^r corresponding to the sphere chain root.

The relation between two successive resolution levels is given by:

$$\begin{aligned} S^{j+1} &= A^{j+1} S^j \\ D^{j+1} &= B^{j+1} S^j \end{aligned} \tag{3}$$

with D^j represents the wavelet detail coefficients of the resolution level (*j*):

$$D^j = \left[D_{j,1} D_{j,2} \dots D_{j,i} \dots D_{j,n_j}\right]^t \quad (4)$$

The A^j and B^j matrices are called the analysis filters of the resolution level *j*.

To reconstruct the superior resolution level we use two matrices P and Q called synthesis filters. The initial resolution level is given by:

$$S^j = P^{j+1} S^{j+1} + Q^{j+1} D^{j+1} \quad (5)$$

The relation between the analysis and synthesis filters is formulated by:

$$[A|B]^t = [P|Q]^{-1} \, then \, [A|B]^t \, [P|Q] = I \quad (6)$$

In order to make a multi-resolution analysis of the spheres based subdivision of the anatomical structure virtual model, we have to compute the filters A^j, B^j, P^j and Q^j for each resolution level (*j*). In the simplest case, the transformation to an inferior resolution level (*j*) of the 3D decomposition of the volumetric model consists in replacing two spheres of the resolution level (*j-1*) by a representative one containing both of them.

The A^j filter is used to select elements of the next inferior resolution level and B^j to extract wavelet coefficients of each level. Hence, the analysis process is formulated by:

$$\begin{aligned} S^r &= A^r S^{r-1} = A^r A^{r-1} \dots A^2 A^1 S^0 \\ D^r &= B^r S^{r-1} = B^r B^{r-1} \dots B^2 B^1 S^0 \end{aligned} \quad (7)$$

Assuming that the initial spheres based decomposition is composed of (2^r) spheres. We have, $S^{(j=0)} = \left[S_{0,2^0} S_{0,2^1} \dots S_{0,i} \dots S_{0,2^r}\right]^t$ with $n_{(j=0)} = 2^r$ and *r* gives the number of levels to reach the coarsest representation corresponding to the spherlet root.

In the case where $r = 3$ (2^3 spheres), we have the TOS approximation and detail vectors given in Table II.

TABLE II. ANALYSIS PROCESS OF A $8 = 2^3$ SPHERES CHAIN

$S^0, D^0 = \emptyset$	S^1, D^1	S^2, D^2	$S^3 = root, D^3$
ϖ_1	ϖ_1	ϖ_1	ϖ_1
ϖ_2	ϖ_2	ϖ_2	$d_2 = \varpi_2 - \varpi_1$
ϖ_3	ϖ_3	$d_3 = \varpi_3 - \varpi_1$	$d_3 = \varpi_3 - \varpi_1$
ϖ_4	ϖ_4	$d_4 = \varpi_4 - \varpi_2$	$d_4 = \varpi_4 - \varpi_2$
ϖ_5	$d_5 = \varpi_5 - \varpi_1$	$d_5 = \varpi_5 - \varpi_1$	$d_5 = \varpi_5 - \varpi_1$
ϖ_6	$d_6 = \varpi_6 - \varpi_2$	$d_6 = \varpi_6 - \varpi_2$	$d_6 = \varpi_6 - \varpi_2$
ϖ_7	$d_7 = \varpi_7 - \varpi_3$	$d_7 = \varpi_7 - \varpi_3$	$d_7 = \varpi_7 - \varpi_3$
ϖ_8	$d_8 = \varpi_8 - \varpi_4$	$d_8 = \varpi_8 - \varpi_4$	$d_8 = \varpi_8 - \varpi_4$

C. Deformable Structures Detection

As in our previous work [22], the first step of the method consists in the precise detection of the gallbladder in the laparoscopic view. First, a deformable particles based model is constructed for each anatomical structure. This is performed by using pre-operative surfacic model of the anatomical structures concerned with the surgical intervention of the gallbladder ablation that have been generated from pre-operative medical image of the gallbladder and surrounding structures. Then, a registration scheme begins with a coarse 2D TOS root detection in the laparoscopic image using the color (C) and spatial (S) models that we have described above. The C-model is used to segment the laparoscopic cholecystectomy images and build the points cloud associated to the anatomical structure (i) which is visible in the step (t) according the surgical workflow of a standard laparoscopic intervention procedure as described in Section 2. The result is the construction of world frame using the relationship between the greatest and most stable parts of anatomical structures such as the liver and the gallbladder. "(1)" gives a pixel wise segmentation of the different structures visible according to the intervention step:

$$P_{C(i,t)}(x_{rgb}) \geq \theta_{rgb} \quad (8)$$

Therefore, we have an initial segmentation of initial of surgical instruments and anatomical structures. However, we observe generally a high correlation between organs ***RGB*** colors in the case of abdominal laparoscopic surgery. As already described above, an ***RGB*** triplet can be found in different regions with low spatial concentration and connectivity. Thus, we propose to use particles swarming to detect and track anatomical structures using the color as well as the spatial distribution.

Particles Swarm Optimization (PSO) is a global search strategy for optimization problems. The first version has been proposed by Kennedy and Eberhart [23] in 1995 and it is based on the social evolution simulation of an arbitrary swarm of particles based on the rules of Newtonian physic. Assuming that we have an N-dimensional problem, the basic PSO algorithm is formulated by position $x_m(t)$ and velocity $v_m(t)$ vectors representing the time evolution of ***M*** particles with random affected initial positions. Hence, we have:

$$x_m(t) = [x_1(t)\, x_2(t) \dots x_N(t)]^T \quad (9)$$

$$v_m(t) = [v_1(t)\, v_2(t) \dots v_N(t)]^T \quad (10)$$

The evolution of the swarm particles in the classical algorithm is done by the following equations:

$$\begin{aligned} v_m(t+1) &= f_{m_i} v_m(t) + f_{m_c} [D_c]_N \left(x_m(t_c) - v_m(t)\right) \\ &\quad + f_{m_s} [D_s]_N \left(x_{opt}(t_s) - v_m(t)\right) \end{aligned} \quad (11)$$

Thus, the new position of the particle *m* is given by:

$$x_m(t+1) = x_m(t) + v_m(t+1) \quad (12)$$

Where $v_m(t)$ and $v_m(t+1)$ are, respectively, the past and the new velocity vectors of the particle m. f_{m_i} is the inertia factor of the particle m, f_{m_c} is its the cognitive factor and f_{m_s} is the social factor. $[D_c]_N$ and $[D_s]_N$ are the N-dimensional diagonal matrices composed of statistically independent normalized random variables uniformly distributed between 0 and 1. t_c is the iteration where the particle m has reached its best position given by x_m. t_s is the iteration where the population has found its best global value given by the coordinates of the particle x_{opt}. It is obvious that particles reach their best local values before that one of them becomes the global best.

The particles swarm optimization method is a meta-heuristic used in combinatorial optimization problems. Its independence from the continuity and gradient information allows

it superior behavior especially in cases where it is impossible to rely on the gradient descent because of discontinuity or hard gradient changes. For this reason, we base our method on the PSO method for the segmentation and tracking of the point clouds generated by the first step of the segmentation process based primarily on knowledge based pixel wise anatomical geometric and color model. As the result of the first step presented previously is a set of disconnected point clouds, it is very difficult if not impossible to apply traditional method such as histogram thresholding, edge detection and even deformable models based segmentation and tracking. In particular, the proposed method is used for the detection of the gallbladder in the video-based laparoscopic cholecystectomy intervention. In the laparoscopic cholecystectomy intervention, the endoscope is focused on the gallbladder so that it is always at the center of the laparoscopic endoscopic image.

The proposed scheme is inspired from the behavior of a swarm of predating eagles. In nature, social eagles swarm construct a circle in the sky around their prey. This is due to the anatomy of their eyes which are symmetric to the axis of the head allowing simultaneous visualization of the prey and the environment around it. In our PSO scheme, each particle in fact represents the left and the right eye of an eagle. For segmentation purposes, we can describe them as the in-eye and out-eye. the In-eye maximizes a set of features concerning the segmented and tracked organ and the Out eye represents the outer organs such as the liver in the case of the laparoscopic cholecystectomy. The In-Eye maximizes the density of ACM color bins defined in the previous of the targeted organ which is in our case the gallbladder. On the other hand, the Out-Eye maximizes the density of the bounding organ which is in this case the liver. Each of the In-Eye and Out-Eye particle are represented by a circle or a square delimiting coarsely the pixels of the respective organs in the endoscopic image. Thus, the two particles are defined using the upper left and the down right pixels in the images. The fitness function has the role of maximizing the density of the targeted organ (gallbladder), minimizing the density of the bounding organ (liver) and reducing the distance between the two particles (In-eye, Out-Eye) all without allowing any collision between them. Thus, this fitness function for the gallbladder as it is the targeted organ becomes

$$F_{gallbladder} = \frac{H}{D} \tag{13}$$

with

$$H = \frac{In - Eye_{density}}{Out - Eye_{density}}, \tag{14}$$

where the density of each particle is given by the ratio between the number of ACM rgb bins and the surface of the particle for each organ (gallbladder, liver). and

$$D = \frac{\|InEye_{center} - OutEye_{center}\|}{InEye_{radius} + OutEye_{radius}}, \tag{15}$$

Here, $(\|.\|)$ denotes the Euclidean distance between the centers of the In-Eye and the Out-Eye particles. This allows to maximize the minimal variance between the targeted structure (gallbladder) and the surrounding structures such as the liver and the covering surgical instruments parts.

The determination of the the points number of the PSO tracking particle of the gallbladder in the laparoscopic view (without calibration) is given with the same manner given in our previous work [22]. Here, we present it for more clarity. the difference is in that, here, we are using a couple of bi-particles one for the inside and other for the outside in extension to our previous work which lies on only one internal particle for hte tracked structure. The number of pixels in each particle is given from the preoperative 3D model based on our previous method [22]. Here, we use the surfacic 3d model of the gallbladder reconstructed using pre-operative images such as ct scan or mri. Assuming the distance between the laparoscope tip (L_{tip}) and the pic of the gallbladder surface (G_{pic}) and assuming that the silouhette of the gallbladder is completely visible in the laparoscopic image, we propose to approximate the gallbladder point cloud by considering the ratio between the half of the surfaci corporal model area (Ω_{gal}) and that of an elementary surface projected into a camera CCD pixel sensor (ω). This ratio is given thus by,

$$\alpha = \frac{\Omega_{gal}}{2 * \omega}, \tag{16}$$

with,

$$\omega = \left| L_{tip}\vec{G}_{pic} \right| \frac{\Omega_{pixel}}{f}, \tag{17}$$

where (Ω_{pixel}) is the area of the pixel in the camera ccd matrix and (f) is the focal length which is the distance between the central point and the image place.

Now, if we consider that the gallbladder is modeled by a set of polygons P_i, we get

$$\Omega_{gal} = \sum_i \Omega_{P_i}, \tag{18}$$

By combining "(17)" and "(18)" in "(16)", α is given so that:

$$\alpha = \frac{f * \sum_i \Omega_{P_i}}{2 * \left| L_{tip}\vec{G}_{pic} \right| * \Omega_{pixel}}, \tag{19}$$

By taking P_i as small as a millimetric surfacic unit, we obtain:

$$\alpha = \frac{f}{2 * \rho^2 * \left| L_{tip}\vec{G}_{pic} \right|} * \nu, \tag{20}$$

where ν is the number of elementary surfaces (surfels) and ρ^2 is the metric area of ccd pixel. Here, we consider it constant during the intervention.

From "(20)", the only measure that is varying during the intervention is $\left|L_{tip}\vec{G}_{pic}\right|$. This is due to the cardiac and the respiratory activities. However, is is generally maintained by the surgical staff as constant and invariant as possible during the whole intervention.

By considering the preoperative medical images (MRI or CT-Scan) exist with millimetric precision, the parameter ν is computed as the length of the segmented gallbladder contour in each tomographic medical image. Assuming that for each preoperative image (i), the gallbladder contour length is given by (Γ_i). Then, "(20)" becomes:

$$\alpha = \frac{f}{2 * \rho^2 * \left|L_{tip}\vec{G}_{pic}\right|} * \Gamma, \tag{21}$$

with

$$\Gamma = \sum_i \Gamma_i, \tag{22}$$

Here, The principal wavelet sphere S_i^0 is projected on the gallbladder area in the 2D laparoscopic image which has the same perimeter as that of the contour of the gallbladder (Γ_i) in the slide (i). Then:

$$\Gamma_i = 2 * \pi * r_i, \tag{23}$$

Given (n) medical imaging slides that cover the target organ and by replacing Γ_i in "(22)" from "(23)", we have:

$$\Gamma = 2 * n * \pi * \sum_{i=1}^{n} r_i, \tag{24}$$

By replacing Γ from "(24)" in "(21)", we get:

$$\alpha = \frac{n * \pi * f}{\rho^2 * \left|L_{tip}\vec{G}_{pic}\right|} * \sum_{i=1}^{n} r_i, \tag{25}$$

By putting

$$\kappa = \frac{n * \pi * f}{\rho^2 * \left|L_{tip}\vec{G}_{pic}\right|}, \tag{26}$$

and

$$P = \sum_{i=1}^{n} r_i, \tag{27}$$

Then, α is given by:

$$\alpha = \kappa * P \tag{28}$$

The internal parameters of the laparoscopic camera are assumed to be invariant during the intervention. the distance between the laparoscope tip and the gallbladder pic can be determined using distance estimation techniques and devices.

V. Experimental Results

To assess the performance of the proposed PSO-based gallbladder detection method in laparoscopic images, we first conduct an experiment on the synthetic image using the method defined in the previous section. Our first synthetic image (Fig. 6) consists of a set of point clouds differing in volume and density. These point clouds represent the possible result of the photometric and textural segmentation step of the gallbladder during the laparoscopic cholecystectomy intervention. Here, the true positive points are those belonging to the greatest cloud positioned in the middle of the image. The points belonging to smaller point clouds or simply black areas around the primary targeted greatest point cloud are either false positive points or true negatives which represent in fact anatomical structures other than the targeted deformable structure which is the gallbladder in our case.

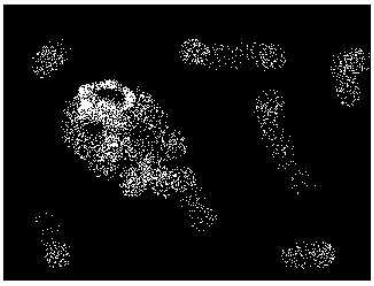

Fig. 6. Synthetic images representing a set of point clouds as the result of photometric and textural segmentation step used to test the PSO-based method.

The PSO-based method is applied to this synthetic image to detect a deformable point cloud representing a gallbladder with no need of explicit initialization of the position of tracking PSO swarm of particles. Initially, the particles are distributed randomly over all the original image. According to the used tracking shapes of the PSO particles (circular or rectangular for instance), each particle is characterized by either the particle's center and radius of the circle or the two points defining the rectangle, namely, the upper left and the lower right corners. In the following experiments, we have used tracking particles with rectangular shapes as this allows to compute efficiently their density by simply comparing the coordinates of the belonging feature points to the rectangle two corners. Next, the intermediate tracking swarm for the synthetic image obtained by applying the PSO-based scheme are shown in Fig. 7 and 8, corresponding to the PSO process application after 10 and 20 iterations, respectively.

The detection result of the major point cloud in the synthetic image using the PSO-based particles is shown in Fig. 9. As expected, we observe that the resulting global particle detects always the major point cloud regardless of the presence of discontinuities due to the large variations of gradient and the existence of neighboring sub-major point clouds of false positives belonging to hypothetically surrounding anatomical structures in the case of a real laparoscopic cholecystectomy image. However, we can observe at this first generation there are some false positives and negatives. this can be heavily

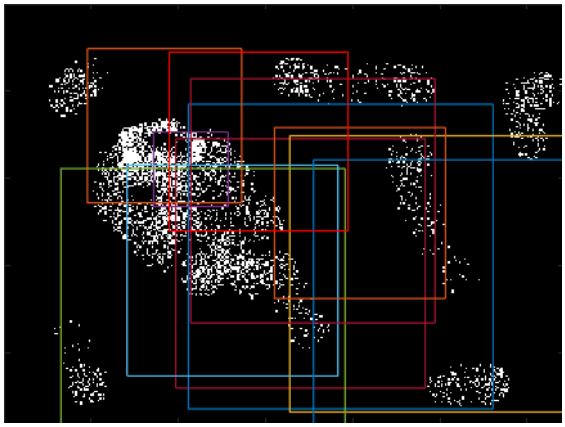

Fig. 7. Intermediate PSO-based tracking swarm of rectangular particles: after 10 iterations.

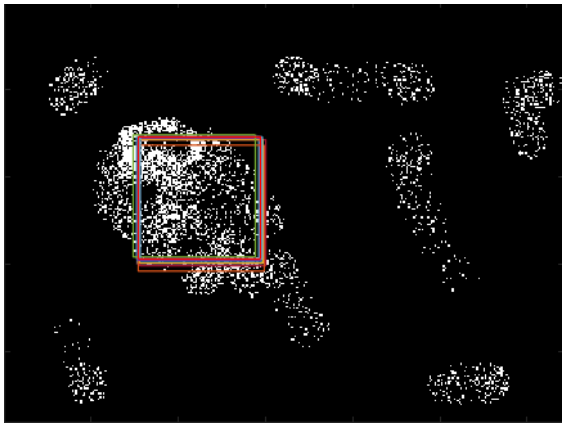

Fig. 8. Intermediate PSO-based tracking swarm of rectangular particles: after 20 iterations.

enhanced by applying a second and third generation detection passes along the boundaries of the first root detection particle.

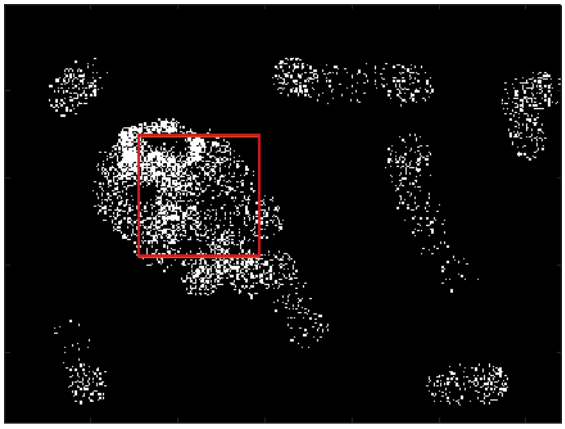

Fig. 9. The detection result of the synthetic image of a deformable structure points' cloud.

The different terms of the PSO-based evolution scheme must be weighted properly to guide the evolving tracking swarm under different image conditions such as those encountered during a laparoscopic cholecystectomy intervention. In the previous experiment on the synthetic image of the points cloud, we have considered the following parameters specific to the PSO-based detection scheme, namely, the size of the tracking swarm expressed by the number of the particles in the population (N=10); The number of the corners of the particle's shape (C=2) as it is a rectangular; the inertial parameters preventing the particles swarm from early collapsing ($W_{min} = 0.3$) and divergence ($W_{max} = 0.9$); the number of iterations of the PSO-based evolution scheme ($It_{max} = 50$); local (c1 = 0.4) and global (c2 = 0.4) PSO parameters which govern the influence of the individual and social terms on the evolution scheme, respectively. In addition, we consider the parameter (α_r) that gives the ratio between the surface of the visible corporal surface of the tacked deformable structure and the size of the image in terms of pixels. Thus, the number of pixels that constraints the size of the particles of the population is given by ($\alpha_p = \alpha_r * \|I\| = 2273$) where $\|I\| = I_L * I_W$ is the resolution of the image in terms of pixels and I_L, I_W are the length and the width of the laparoscopic image, respectively. The graphs represent the position, size and density of the global best particle of the population to segment and detect the deformable structure point cloud along time (PSO evolution iterations, $It_{max} = 50$). As it can be seen (Fig. 10), the tracking swarm stabilizes after only 20 iterations.

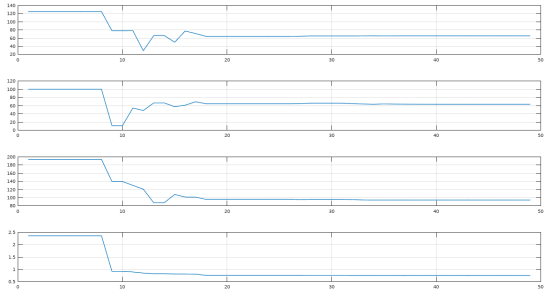

Fig. 10. Evolution of the best global particle of the population over time.

VI. Conclusion

In this paper, we have proposed a new automatic segmentation and tracking method of deformable structures in a minimally invasive surgery intervention such as laparoscopic cholecystectomy. The segmentation of anatomical structures is performed thanks to a modified PSO scheme to segment and track the deformable structure during the intervention, namely, the gallbladder in the case of laparoscopic cholecystectomy. The reconstructed 3D model is analyzed using a wavelet based method to perform the registration task. Therefore the system is able to track surgical instruments with possible interactive update of the color model guided by a priori anatomical knowledge. The only drawback of the proposed system is the need of the determination of a precise distance between the endoscope tip and the closest point of the corporal surface of the tracked anatomical structure. We are working on the development of such device to estimate precisely this distance. We intend to verify the effectiveness of the proposed method first on 3d printed deformable phantoms corresponding to real patients before testing the performance of the system intra-operatively.

VII. Conflict of Interest Disclosure

The author(s) declare(s) that there is no conflict of interest regarding the publication of this paper.

References

[1] R. Azuma, Y. Baillot, R. Behringer, S. Feiner, S. Julier, and B. MacIntyre, "Recent advances in augmented reality," *Computer Graphics and Applications, IEEE*, vol. 21, no. 6, pp. 34–47, 2001.

[2] R. Azuma *et al.*, "A survey of augmented reality," *Presence-Teleoperators and Virtual Environments*, vol. 6, no. 4, pp. 355–385, 1997.

[3] W. Reynolds, "The first laparoscopic cholecystectomy," *JSLS, Journal of the Society of Laparoendoscopic Surgeons*, vol. 5, no. 1, pp. 89–94, 2001.

[4] L. W. Traverso, "Carl langenbuch and the first cholecystectomy," *The American Journal of Surgery*, vol. 132, no. 1, pp. 81–82, 1976.

[5] L. Soler, S. Nicolau, J.-B. Fasquel, V. Agnus, A. Charnoz, A. Hostettler, J. Moreau, C. Forest, D. Mutter, and J. Marescaux, "Virtual reality and augmented reality applied to laparoscopic and notes procedures," in *ISBI*, 2008.

[6] K. G. Vosburgh and R. S. J. Estepar, "Natural orifice transluminal endoscopic surgery (notes): an opportunity for augmented reality guidance," *Studies in health technology and informatics*, vol. 125, p. 485, 2006.

[7] S. Connor and O. Garden, "Bile duct injury in the era of laparoscopic cholecystectomy," *British journal of surgery*, vol. 93, no. 2, pp. 158–168, 2006.

[8] J. Cullen, "Laparoscopic cholecystectomy: Avoiding complications," in *The SAGES Manual*. Springer, 2006, pp. 140–144.

[9] S. Cawich, D. Mitchell, M. Newnham, and M. Arthurs, "A comparison of open and laparoscopic cholecystectomy done by a surgeon in training," *West Indian Medical Journal*, vol. 55, no. 2, pp. 103–109, 2006.

[10] L. KOZUMPLÍK, "New classification of major bile duct injuries associated with laparoscopic cholecystectomy," *Scripta Medica (Brno)*, vol. 75, no. 6, pp. 283–290, 2002.

[11] G. S. Litynski, "Erich muhe and the rejection of laparoscopic cholecystectomy (1985): a surgeon ahead of his time," *JSLS, Journal of the Society of Laparoendoscopic Surgeons*, vol. 2, no. 4, pp. 341–346, 1998.

[12] R. Haluck, "Laparoscopic surgical instrument and method," 2003.

[13] T. Blum, H. Feußner, and N. Navab, "Modeling and segmentation of surgical workflow from laparoscopic video," *Medical Image Computing and Computer-Assisted Intervention–MICCAI 2010*, pp. 400–407, 2010.

[14] A. Jacquot, P. Sturm, and O. Ruch, "Adaptive tracking of non-rigid objects based on color histograms and automatic parameter selection," in *Application of Computer Vision, 2005. WACV/MOTIONS'05 Volume 1. Seventh IEEE Workshops on*, vol. 2. IEEE, 2005, pp. 103–109.

[15] S. Nicolau, X. Pennec, L. Soler, X. Buy, A. Gangi, N. Ayache, and J. Marescaux, "An augmented reality system for liver thermal ablation: Design and evaluation on clinical cases," *Medical Image Analysis*, vol. 13, no. 3, pp. 494–506, 2009.

[16] H. Kato, "Artoolkit: Library for vision-based augmented reality," *IEICE, PRMU*, pp. 79–86, 2002.

[17] D. Wagner and D. Schmalstieg, "Artoolkitplus for pose tracking on mobile devices," in *Proceedings of 12th Computer Vision Winter Workshop (CVWW'07)*, 2007, pp. 139–146.

[18] S. Nicolau, X. Pennec, L. Soler, and N. Ayache, "An accuracy certified augmented reality system for therapy guidance," *Computer Vision-ECCV 2004*, pp. 79–91, 2004.

[19] ——, "Evaluation of a new 3d/2d registration criterion for liver radiofrequencies guided by augmented reality," *Surgery Simulation and Soft Tissue Modeling*, pp. 1001–1001, 2003.

[20] D. E. Litwin and M. A. Cahan, "Laparoscopic cholecystectomy," *Surgical Clinics of North America*, vol. 88, no. 6, pp. 1295–1313, 2008.

[21] M. Feuerstein, "Augmented reality in laparoscopic surgery : New concepts for intraoperative multimodal imaging," Ph.D. dissertation, Technische Universitt Mnchen, 2007.

[22] H. Djaghloul, M. Batouche, and J.-P. Jessel, "Automatic pso-based deformable structures markerless tracking in laparoscopic cholecystectomy," in *Hybrid Artificial Intelligence Systems*. Springer, 2010, pp. 48–55.

[23] J. Kennedy, R. Eberhart *et al.*, "Particle swarm optimization," in *Proceedings of IEEE international conference on neural networks*, vol. 4, no. 2. Perth, Australia, 1995, pp. 1942–1948.